Pergamon

Journal of Asian Earth Sciences, Vol. 16, Nos. 2-3, pp. 239–252, 1998

Printed in Great Britain
1367-9120/98 $ - see front matter

PII: S0743-9547(98)00002-6

The Namche Barwa syntaxis: evidence for exhumation related to compressional crustal folding

Jean-Pierre Burg*¶, Peter Nievergelt*, Felix Oberli*, Diane Seward*, Philippe Davy†, Jean-Christophe Maurin‡, Zhizhong Diao§ and Martin Meier*

*Department Erdwissenschaften, ETH-Zentrum, Sonneggstrasse 5, CH-8092 Zürich, Switzerland,
†Géosciences Rennes, Campus Beaulieu, Avenue Général Leclerc, F-35042 Rennes cédex, France,
‡Institut de Physique du Globe, 5, rue R. Descartes, 67084 Strasbourg cédex, France and
§Chengdu Institute of Geology and Mineral Resources, 82/3 n° 1 Ring Road (N), Chengdu 610082, P.R. China

(*Received* 12 *June* 1997; *accepted* 12 *January* 1998)

Abstract—Geological observation in the eastern end of the Himalayas shows that the Asia/India suture is folded and continues southward into India and Burma where the continuation of the Transhimalayan plutonic complex can be identified. Metamorphic rocks derived from India occur structurally below the suture, in the core of a regional antiform. Isotopic and fission track dating are consistent with the geological interpretation. In addition, they establish cooling exhumation of rocks from *c.* 30 km depth within the last 4 Ma. Rapid exhumation of deep crustal levels in mountain systems is generally related to extension subsequent to thermal softening of a thickened continental lithosphere. However, in the Eastern Himalayas, we argue that exhumation is caused by *c.* 10 mm yr^{-1} erosion coeval with crustal scale folding. The general history of this syntaxis resembles the evolution of the western Himalayas syntaxis in Pakistan.

Introduction

The Himalayas terminate at both ends in syntaxes (Wadia, 1931), a distinctive feature of collisional belts (e.g. the Alps, the Caribbean) where orogenic structures seem strongly bent around a vertical axis. Although little documented, the eastern syntaxis of the Himalayas, named Namche Barwa after the 7756 m high peak that towers it, is traditionally regarded as symmetrical to the Nanga Parbat syntaxis, the western bend of the Himalayas in Pakistan (Wadia, 1931; Gansser 1991). Indeed, on topographic maps and space images of the area, the Namche Barwa peak seems to mark the vertical axis of a 180° bend of the Himalayan structural trends, giving rise to the U-turn of the Yalu Tsangpo (Brahmaputra) River. Geologists have therefore inferred that there would be a bent segment of the Palaeocene Tethyan suture zone around the Namche Barwa (Wadia, 1957; Gansser, 1966, 1980, 1991). Chinese exploratory studies have resulted in a geological map displaying a variety of undifferentiated migmatitic gneisses of Proterozoic age (Institute of Geology and Mineral Resources and Chinese Academy of Geological Sciences 1988). Interpretation of Landsat and Spot satellite images extended our field observations to prepare a geological sketch map based on lithology distribution and structure orientation (Fig. 1). Analytical results include microstructural work to relate deformation and metamorphism, along with geochronology to constrain the timing and rates of development of this end of the Himalayas. In this contribution we wish to extend a report where first results and a hint at their interpretation in terms of a fast growing, crustal scale antiform have been introduced (Burg *et al.*, 1997). The crustal antiform folds the Yalu Tsangpo segment of the Tethyan suture into a sharp "syntaxis" mirroring the western syntaxis of the Himalayas, around the Nanga Parbat mountain. Having documented the main tectonic units in the Namche Barwa area, we will discuss the southeastward continuation of the Tethyan suture into India and Burma.

Lithologies: Trans-Himalayan and Indian crustal segments

Paleozoic and Mesozoic quartzites, quartzphyllites, shales and marbles that screen calc alkaline plutons of the Transhimalayan plutonic belt (Gansser, 1980, Burg *et al.*, 1983) wrap around the Namche Barwa area proper (Fig. 1). The sediments become penetratively deformed and metamorphosed towards contact with dykes and plutons and the metamorphic grade reaches regional anatexis in the northeastern, eastern and southeastern, structurally deeper regions. Between Nyingchi and Parlung (Fig. 1) migmatites may include pre-Carboniferous series that have been intruded by dykes and plutons of gabbroic to granodioritic composition, one of which is dated at *c.* 73 Ma (U–Pb zircon, Zhang *et al.*, 1981). Andalusite and sillimanite characterise a high temperature–low pressure metamorphic terrane (Wang, 1985; Chang *et al.*, 1992) similar to

¶ Corresponding author: Telephone: (41) 1-632-6027; Telefax: (41) 1-632-1030 and -632-1080; e-mail: jpb@erdw.ethz.ch.

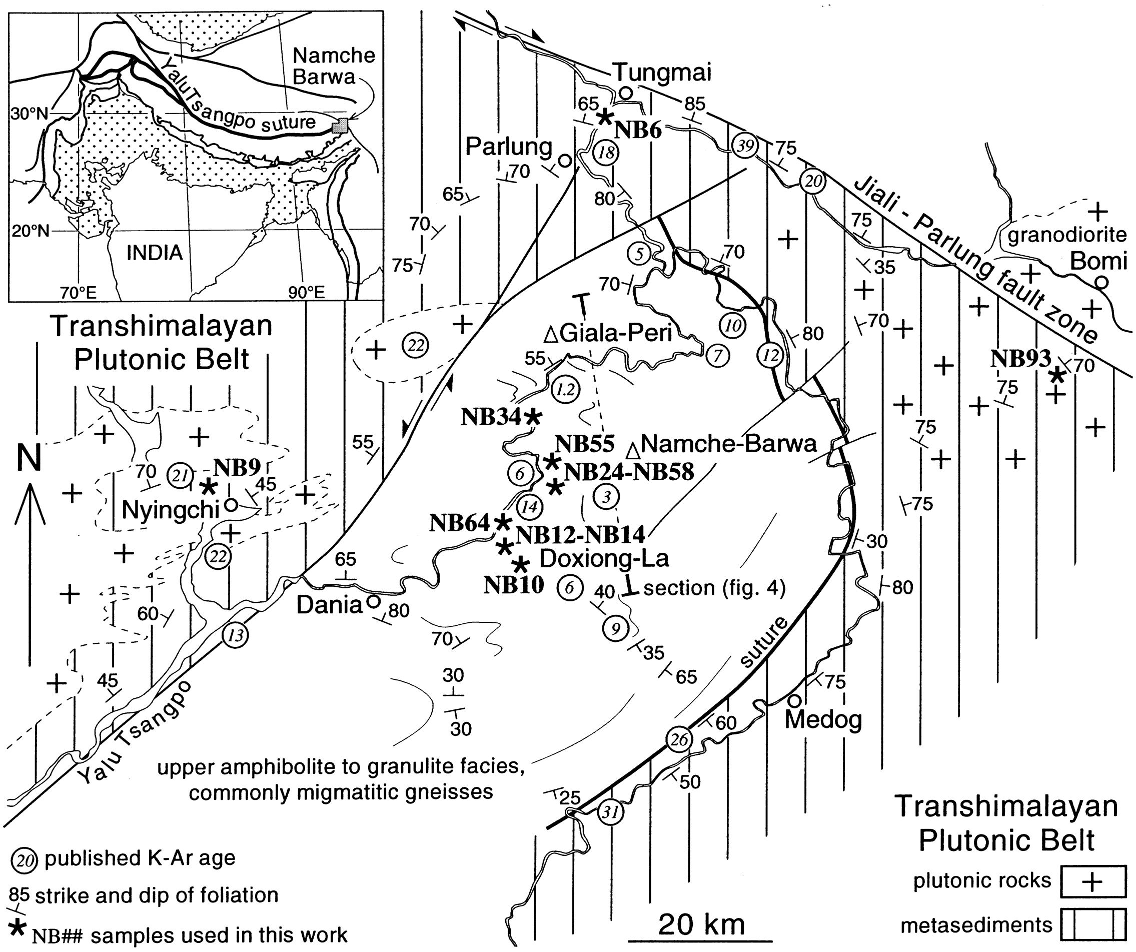

Fig. 1. Simplified geological map of the Namche Barwa area (situated in the Himalayas—Tibet orogenic system, in inset (from Burg *et al.*, 1997). K–Ar ages are published by Group of K–Ar Geochronology *et al.* (1979), Zheng and Chang (1979), Zhang *et al.* (1981 and 1987) and Ratschbacher *et al.* (1992).

those known in the belt, further west (Burg *et al.*, 1987).

In the core of the syntaxis, and structurally below the Transhimalayan plutonic belt, rocks are dominantly layered quartz–feldspar–biotite gneiss with a migmatitic character. Amphibole, seldom muscovite, occasional garnet and fibrolitic sillimanite are part of the assemblage. Metamorphic layering ranges from dm to a few tens of m, often with sharp boundaries, but cauliflower structures (Fig. 2) suggest that it was subhorizontal during anatexis, before being tilted to the present-day attitude. Cross-cutting leucosomes locally parallel to the axial traces of folds that fold the metamorphic layering (Fig. 3) indicate that anatexis has lasted longer than the main fabric development. The banded migmatitic gneiss series comprises mafic, pelitic and rare carbonate intercalations along with sporadic ultramafites (Wang, 1985; Chang *et al.*, 1992). This sequence is strongly reminiscent of the similar sequence known in granite and gneiss domes of the North Himalayan belt (Burg and Chen, 1984; Burg *et al.*, 1987) but we have recorded no undeformed felsic intrusions in this part of the Namche Barwa area. Dykes of leucogranite and tourmaline-rich pegmatite within the layered migmatites and associated gneiss have been found in a reconnaissance section to the west, south of Dania (Fig. 1).

Along the northeastern and southeastern segments of the syntaxis, a pervasively reactivated mylonitic zone with lenses of metabasites and serpentinites separates the Transhimalayan rocks from the core migmatites (Fig. 1). The basic–ultrabasic lenses suggest that this boundary is the eastern continuation of the Yalu Tsangpo suture, with remnants of meta-ophiolites, folded around the Indian-derived core migmatites. The northwestern contact between the Transhimalayan rocks and the core migmatites is a brittle, sinistral fault zone (Fig. 1).

Antiformal structure

Folding

The large-scale structure is a 30 to 40 km wide antiform whose hinge lies near Doxiong-La. Its northern limb is dominated by large parasitic folds such as the tight, north- to north-east facing anticline that builds the Namche Barwa peak proper (Fig. 4). Dips of foliation planes, vergence of mesoscopic folds and the lithologies of pebbles that come indisputably from the Giala Peri peak suggest that it contains an antiform equivalent to the Namche Barwa anticline. The southern limb appears less tightly folded, being nearly homoclinal on a regional-scale section (see also Zheng

Fig. 2. To the right of the hammer, cauliflower structures (Burg, 1991) in migmatites, near NB55 (Fig. 1).

and Chang, 1979; Liu, 1984). Bending around the syntaxis is reflected by regular changes in strike of the usually $>70°$ dipping foliations of the Transhimalayan sequences (Fig. 1).

Metamorphic layering contains, and is parallel to, the main-phase foliation and most lithological boundaries are transposed into these planes. They both result from polyphase, intense deformation, including isoclinal folding parallel to the mineral and stretching lineation contained within the main fabric surface where recrystallisation has preserved the lineation. Planar and linear structures are deformed by several sets of folds that occur at all scales and are fundamentally parasitic to the large-scale antiform. Axes of post-foliation, open to isoclinal folds with a variable apparent vergence trend N100 to N130 in the core Doxiong-La area where they seldom plunge more than 50°E and/or W. Axes of identical short wavelength, large amplitude folds rotate into a NNE direction towards the northeastern, external part of the antiform, around Parlung, where they have nearly vertical plunges. In this region, poles to foliation consistently fit around a fold axis plunging more than 60°, roughly to the N (Fig. 5). Folds are strongly disharmonic (Fig. 6), which seems to be responsible for the large "crocodile-type" wedge of foliations seen in the Namche Barwa western face (Fig. 4). The disharmonic geometry of the commonly regular fold-trains displays hanging wall layers systematically more amplified, i.e. more shortened than footwall layers, which points to a compressional origin of folding. Main folding has preceded several sets of kinks, crenulations and shear bands. Because of the abundant and tight post-foliation folds, the original direction of the main-phase lineation is difficult to ascertain. It roughly trends NNE on gently dipping foliation planes of the hinge region. Weakly developed shear bands form an S-C-type fabric that suggests bulk SSW-ward flow during the earliest-identified, syn-migmatitic deformation event, which is consistent with the subduction direction of India under the Transhimalayan belt (Chang *et al.*, 1977; Allègre *et al.*, 1984; Dewey *et al.*, 1988).

Many late, ductile to semi-brittle shear bands formed at lower amphibolite and upper greenschist facies (stable biotite). These shear bands indicate an overall external-side (with respect to the core of the antiform) down displacement and accommodate local strain in hinge regions.

Faulting

Faults, marked by several centimetre thick gouges and brecciated zones, are abundant and recent activity is confirmed by the presence of hot springs along the fault zones (Chang *et al.*, 1992). The NE–SW sinistral fault that cuts the northwestern side of the antiform is

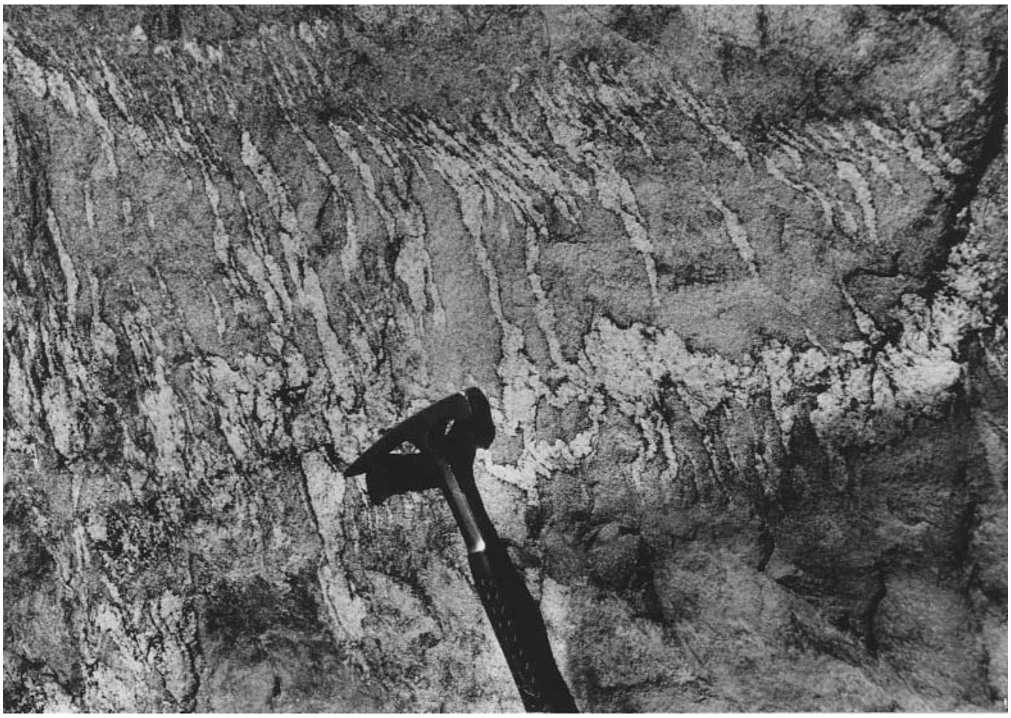

Fig. 3. Leucosome veins along the axial trace of late folds in migmatites; same site as Fig. 2.

a wide crushed zone marked by a complex set of dominantly sinistral and minor north-northwestward reverse striated planes. It offsets the ophiolite bearing suture by *c.* 60 km. Back-thrusting known along the Yalu Tsangpo suture to the west (Burg and Chen, 1984, Ratschbacher *et al.*, 1992) seems to be minor to the east of the sinistral fault zone. It is possible that back-thrusting is partly taken up by the syntaxis antiform, the fault assuming a transfer role from thrust dominated to fold dominated back-vergent convergence.

The syntaxis is cut at its northeastern tip by the active dextral Jiali-Parlung fault (Armijo *et al.*, 1986). The fault (Fig. 1) is actually a *c.* 1 km wide zone in which many subvertical, WNW–ESE foliation planes have been reactivated by dextral slip as documented by slickenside striations. Dextral slip on WNW–ESE planes and sinistral slip on SW–NE planes are conjugate (Ratschbacher *et al.*, 1992).

Microfault planes were systematically measured around and within the core of the syntaxis. The computer-aided method designed by Etchecopar *et al.* (1981) has been applied to calculate local orientations of principal stress axes ($\sigma_1 \geqslant \sigma_2 \geqslant \sigma_3$) and shape ratios of paleostress ellipsoids [$R = (\sigma_2 - \sigma_3)/(\sigma_1 - \sigma_3)$]. Most of the calculated stress tensors indicate reverse strike-slip or transpression with a horizontal compressive maximum stress σ_1, a vertical minimum or intermediate stress σ_2 close to σ_3 and an R ratio ranging from 0 to 0.25. Regionally distributed examples are given in Fig. 7. Two main characteristics can be emphasised. First, the σ_1 compression direction regionally trends N–S to N160°E but exhibits a conspicuous counterclockwise deflection to NW–SE along the northeastern edge of the syntaxis. This deflection is related to the Jiali-Parlung fault. Second, perturbations of the stress regime from pure compressive to constrictive along the northwestern border of the syntaxis are due to a corner effect in a restraining bend along the reverse strike-slip fault that offsets the suture. Our fault analysis is consistent with the present-day compression direction derived from the modern seismicity (Holt *et al.* 1991, Wu 1992). Earthquakes with magnitude $\geqslant$8, frequently with $M_s = 6$–6.9, occur in this area. Fault plane solutions account mainly for SW–NE sinistral strike slip faulting and roughly northward thrusting (Chang *et al.* 1992), compatible with observed fault planes.

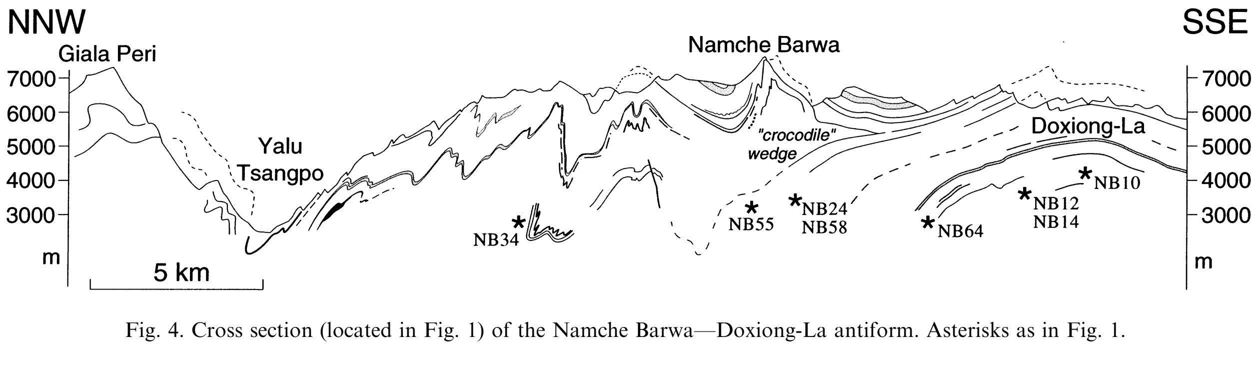

Fig. 4. Cross section (located in Fig. 1) of the Namche Barwa—Doxiong-La antiform. Asterisks as in Fig. 1.

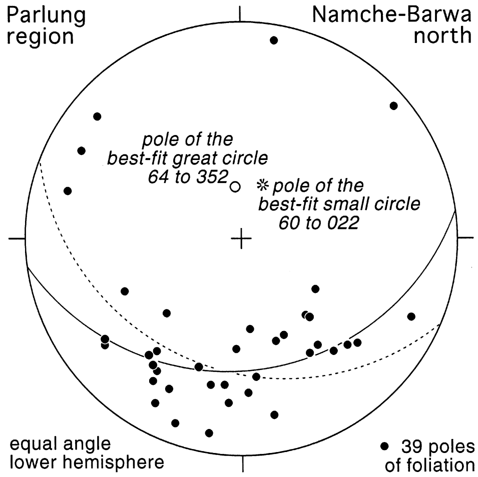

Fig. 5. Great circle (solid line) and small circle (dashed line) for determination of the main antiform axis that folds foliations in the Parlung region.

Metamorphic history

We concentrate our discussion on the core area and do not document the high temperature–low pressure metamorphic sequences of the Transhimalayan plutonic belt.

Retrograde greenschist overprint was detected only from local growth of actinolite, epidote and chlorite in cracks and fractures and occurs in the reworked serpentinite bearing mylonitic suture. These metamorphic temperatures range between 430–480°C and pressures between 5.5–6.5 Kbar (Wang, 1993). Because it is localised, this late retrogression is considered to have had no effect on the mineral compositions of metapelites and garnet-amphibolites which were chosen to estimate earlier metamorphic conditions. These deepest levels also include spinel-olivine-calcite and diopside-garnet marbles and a variety of calcsilicate layers and pods. The NB14 gneiss sample contains relic garnet and ferrohypersthene (Table 1) hinting at early granulite facies conditions. Small bodies of spinel-bronzite-forsterite (Fo_{75})–magnesio-hornblende (50% modal composition) ultramafic rocks represent lenses of recrystallised olivine- and opx-hornblendites (NB55, Table 1). They are interpreted as high-pressure basic granulites by Zhong and Ding (1996).

Highest metamorphic conditions have been measured on the NB24 metapelite, a boulder collected in a creek at the western foot of the Namche Barwa peak (Fig. 1). Electron microprobe analyses (Table 1) show chemical zoning of garnet to be minimal. Temperature and pressure for equilibrium are 720–760°C and 8–10 Kbar (Fig. 8). We do not accept the higher pressures put forward by Liu and Zhong (1997) who used 2-feldspar thermobarometry, which is subject to considerable uncertainties, and who did not use compositions of minerals in actual equilibrium. The transformation of kyanite into sillimanite (see also Liu and Zhong, 1997) and occasionally andalusite is consistent with decompression witnessed by breakdown of garnet and kyanite into a spinel-plagioclase symplectite (Fig. 9). These mineral phases have equilibrated at 550–650°C and 7–8 Kbar. The layered migmatites display consistent assemblages of quartz-feldspar-biotite, often hornblende, seldom muscovite and occasionally fibrolitic sillimanite and/or garnet. Leucosomes contain biotite and cordierite.

Estimates obtained from fresh garnet-amphibolites in migmatites (NB34 in Fig. 1, mineral compositions in Table 1) yield $T > 600$°C and $P > 8$ kb (Fig. 8). In

Fig. 6. Disharmonic fold in the migmatites, near NB64 (Fig. 1).

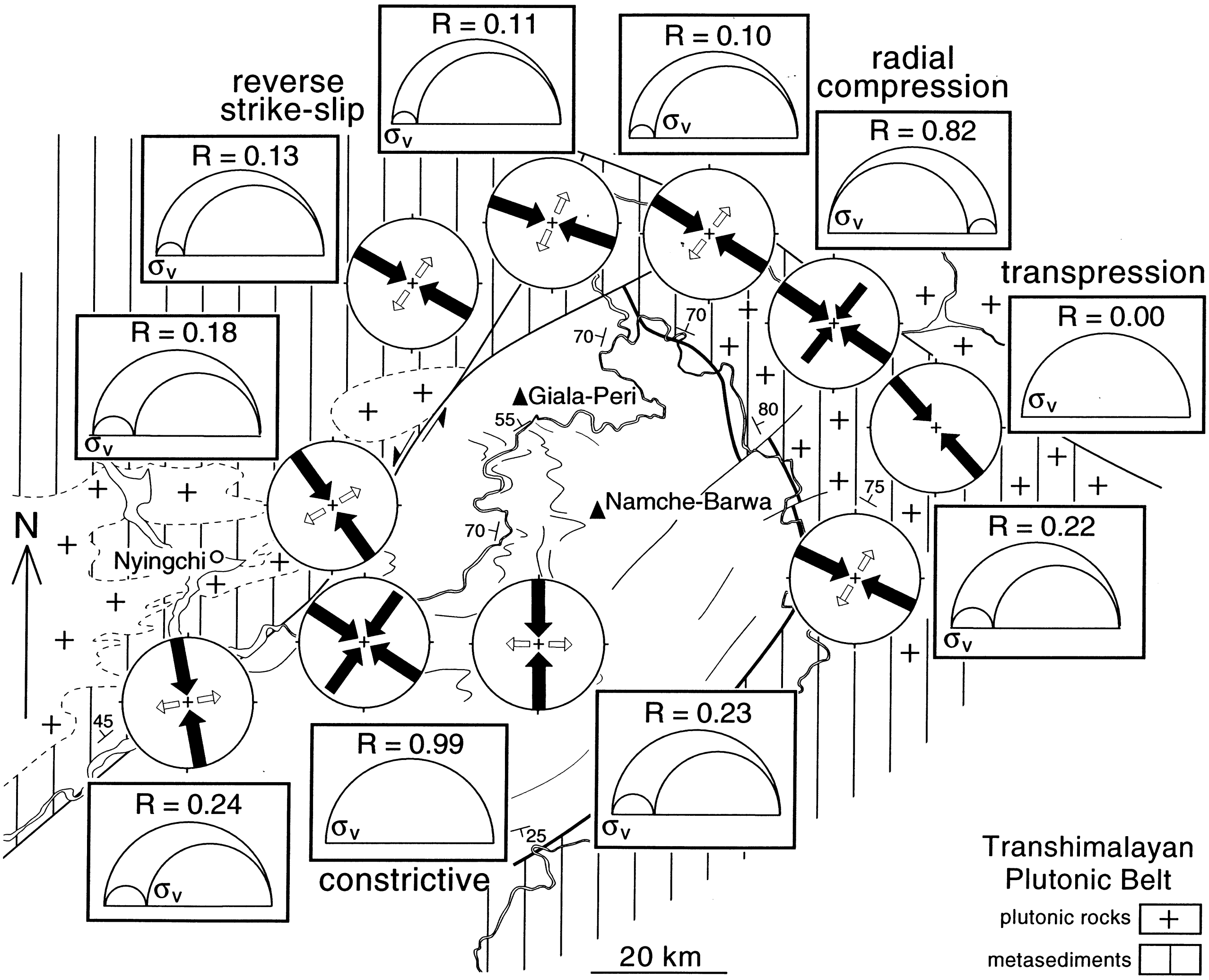

Fig. 7. Stress tensors around and within the Namche Barwa syntaxis.

Table 1. Composition of representative minerals in different rock types: NB 14 hornblende gneiss, NB55 ultramafic rock, NB34 amphibolite, NB24 and NB58 metapelites, (see text)

wt.%	NB 14 Opx	NB 14 Plag	NB 55 Oliv	NB 55 Gar	NB 55 Amph	NB 34 Gar	NB 34 Amph	NB 34 Plag	NB 24 Gar	NB 24 Bio	NB 24 Plag	NB 24 Spinel	NB 58 Gar
SiO_2	50.13	46.53	37.62	40.01	48.47	38.78	41.28	52.34	38.06	35.65	56.09	1.70	37.86
TiO_2	0.09	—	—	—	0.60	0.05	1.81	—	—	5.39	—	—	—
Al_2O_3	1.13	33.92	—	22.95	9.95	20.40	12.40	30.78	21.77	17.44	27.89	59.45	21.66
Cr_2O_3	0.07	—	—	0.42	0.48	—	0.10	—	—	0.06	—	0.11	—
Fe_2O_3	0.51	0.44	—	1.15	4.96	1.43	3.63	—	1.08	—	0.45	—	1.28
FeO	31.04	—	25.04	17.09	1.97	24.90	15.77	0.44	30.59	16.88	—	29.68	33.63
MnO	0.76	—	0.41	0.87	0.08	1.23	0.20	—	1.78	0.11	—	0.16	0.36
MgO	15.26	—	37.57	12.30	17.41	4.19	8.23	—	5.32	10.94	—	5.53	5.32
CaO	0.63	17.40	—	6.12	12.49	9.96	11.39	13.26	2.79	—	10.16	0.05	1.22
Na_2O	—	1.64	—	—	0.82	—	1.52	3.86	—	0.16	6.00	0.15	0.04
K_2O	—	—	—	—	0.23	—	1.42	0.14	—	9.23	0.15	—	0.01
NiO	0.06	—	0.09	0.08	0.11	—	—	—	—	0.08	—	0.12	—
H_2O calc.	—	—	—	—	2.13	—	1.98	—	—	3.89	—	—	—
Total	99.68	99.93	100.73	100.99	99.69	100.94	99.73	100.82	101.39	99.83	100.74	96.95	101.38
	Wo 0.01	An 0.86	Fo 0.72	Gr 0.12	Magnesio	Gr 0.23	Ferroan	An 0.65	Gr 0.04		An 0.48	MgSpi 0.25	Gr 0.0
	En 0.44	Ab 0.14	Fa 0.27	Al 0.36	Hornbl.	Al 0.54	Pargasit.	Ab 0.34	Al 0.67		Ab 0.51	FeSpi 0.75	Al 0.75
	Fs 0.50			Py 0.46		Py 0.16	Hornbl.	Or 0.01	Py 0.21		Or 0.01		Py 0.21
	Px 0.01			Sp 0.02		Sp 0.03			Sp 0.04				Sp 0.0
						An 0.04							An 0.04

Electron microprobe analyses with CAMECA SX 50 on-line PAP correction procedure. Single measurements not detected or smaller than 0.05. Garnet calculated on basis of 12 O. Amphibole recalculated on basis of 23 O and 13 cations +K + Na (classification according to Leake, 1978)

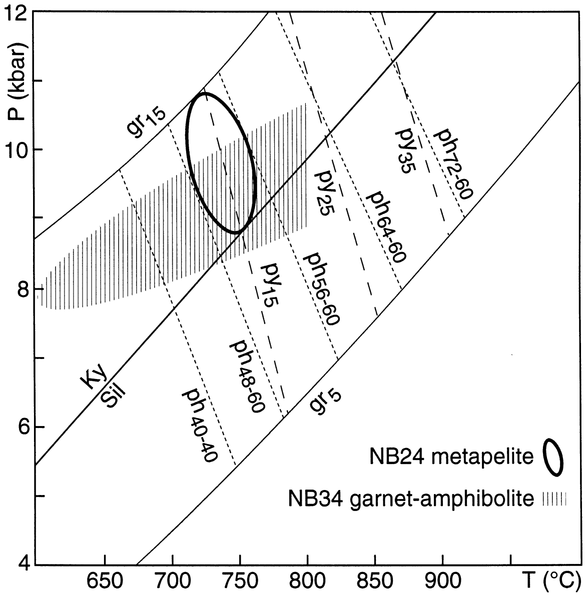

Fig. 8. Earliest metamorphic conditions estimated from phase equilibria (Connolly 1990) in kyanite-biotite-Kfeldspar-plagioclase-quartz-rutile metapelites and garnet amphibolites. gr## = grossular content; pyr = pyrope content; ph## = phlogopite content. Ky = kyanite and Sil = sillimanite.

other amphibolites of the core region, decompression has produced breakdown of garnet to amphibole-plagioclase, locally to pyroxene-plagioclase symplectite. In ultramafic rocks (NB55, Table 1) decompression has produced breakdown of garnet $Gr_{12}Al_{36}Py_{46}Sp_2$ to orthopyroxene-spinel-hornblende symplectite. Incipient breakdown of hornblende with quartz to pyroxene and plagioclase is also textural evidence for decompression rather than a prograde reaction in the transition zone to granulite conditions.

Geochronology

In the Transhimalayan rocks, conventional K–Ar ages derived from micas fall between 39 and 18 Ma, contrasting with dates younger than 14 Ma and as young as 1.2 Ma within the core migmatitic gneisses (Fig. 1). These ages refer to the times when the different crustal segments cooled to temperatures less than *c.* 300°C (Harrison *et al.*, 1985) and point to young thermotectonic activity in the core of the Namche Barwa antiform. To corroborate these young low-temperature ages, we document zircon and apatite fission-track data from three layered gneisses taken in the core of the antiform, at elevations of 2900 m (NB64), 3730 m (NB12) and 4100 m (NB10, Figs 1 and 4). In order to extend the geochronological information to the higher temperature range, we summarise single-crystal U–Th–Pb results on xenotime (NB12) and

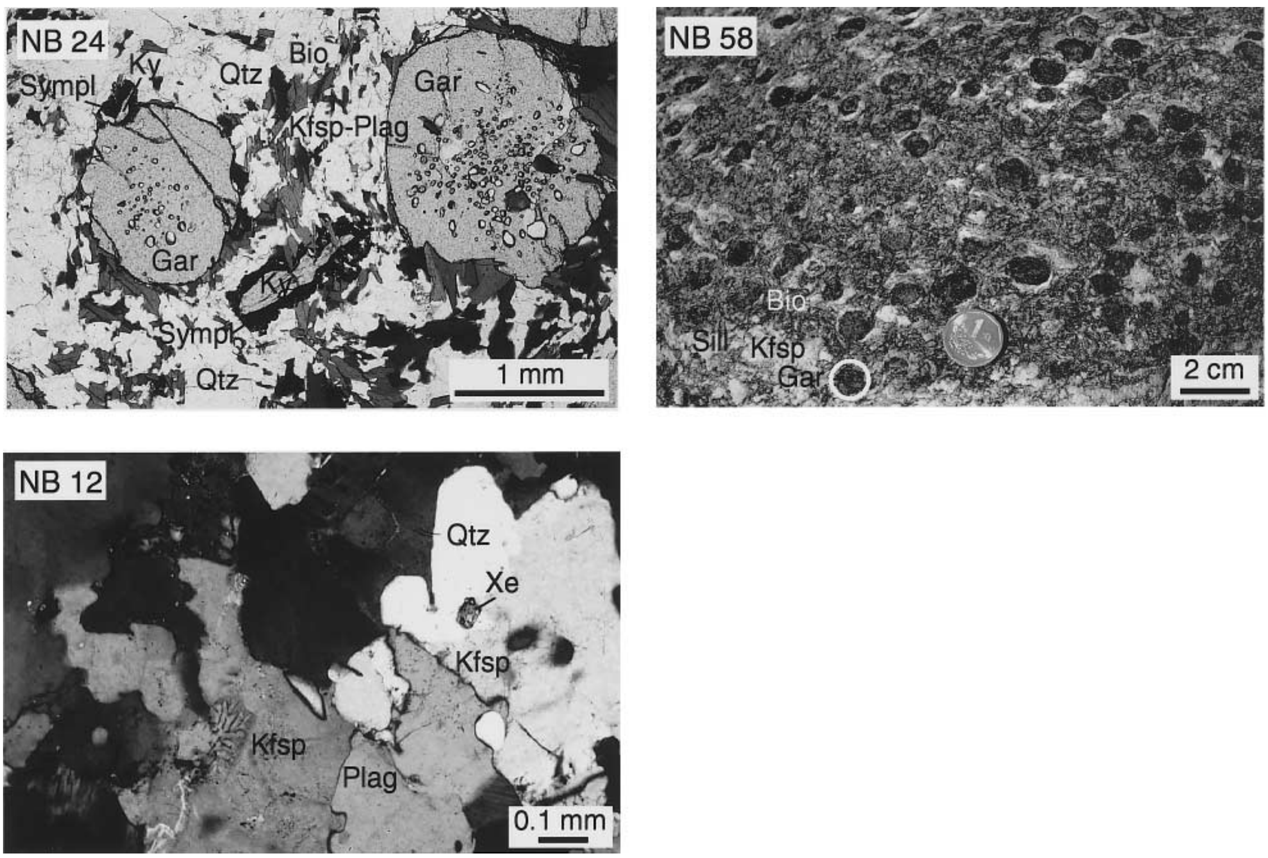

Fig. 9. (NB24). Photomicrograph of the metapelite used for P-T estimation given in Fig. 8, same abbreviations as Fig. 8 with typically garnet (Gar), K-feldspar (Kfsp), plagioclase (Plag), biotite (Bio) and kyanite (Ky) with symplectite rim of plagioclase and spinel (Sympl); Qtz = quartz. (NB58). Field photo of the NB24–NB58 metapelite block with up to 1 cm large sillimanite (Sil) aggregates and relictual kyanite; other abbreviations as for NB24. (NB12). Xenotime (Xe) in the migmatitic layered leucosome.

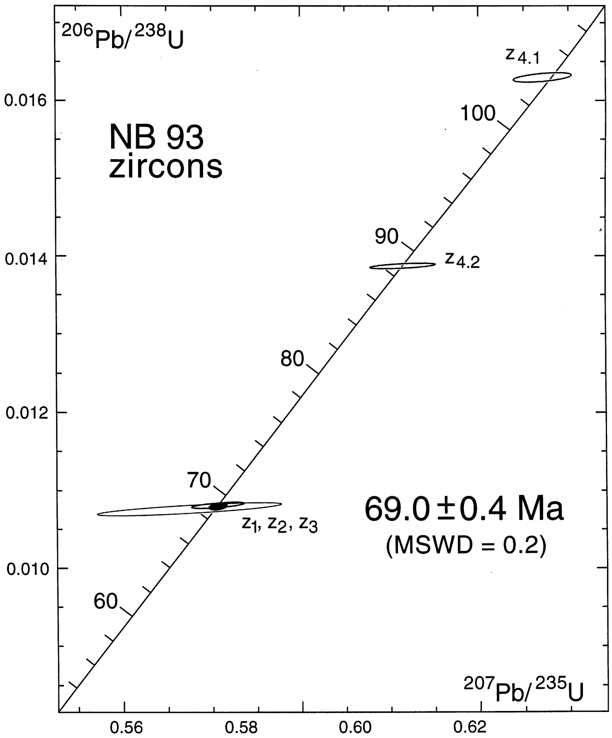

Fig. 10. Conventional Concordia representation of single crystal zircon results for NB93 (northeastern region, Fig. 1); 95% confidence level based on internal errors.

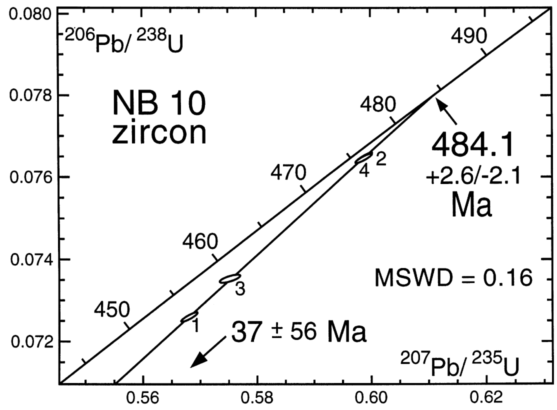

Fig. 11. Conventional Concordia representation of single crystal zircon for NB10 (near Doxiong-La, Fig. 1); 95% confidence level based on internal errors.

thorite (NB64), and present new Sm–Nd data on garnet and whole rock for metapelite sample NB58. Primary ages of major lithologies are obtained by U–Pb single-zircon measurements for the NB10 orthogneiss (near Doxiong-La) and for the NB93 granodiorite (south of Bomi, Fig. 1). A more comprehensive account of the isotopic data will be given elsewhere (Oberli *et al.* in preparation).

Primary ages of major lithologies

Transhimalayan terrain: NB93 is a granodiorite intrusive in amphibolite facies metasediments, all pertaining to the east-peripheral sequences which we regard as the southeastward continuation of the Transhimalayan plutonic belt (Fig. 1). Data from two abraded and one only slightly abraded zircon grains form a tight cluster on Concordia curve and yield a weighted mean $^{206}Pb/^{238}U$ age of 69.0 ± 0.4 Ma (Fig. 10, Table 2), which we interpret to closely approximate the age of intrusion. Two abraded fragments from a fourth grain (z_4) give analytically concordant results, but plot at apparent $^{206}Pb/^{238}U$ ages of 88.8 and 104.3 Ma, respectively. These older ages point to the entrainment of zircon xenocrysts that may have been partially overgrown or reset by magmatic processes, given that the presence of this grain in the sample is not due to laboratory contamination. Ages of these xenocrystic components suggest that the granodiorite has intruded a relatively young, possibly Cretaceous crust. This as well as the 69 Ma age of the granodiorite is consistent with published intrusion ages for the Transhimalayan plutonic belt that span *c.* 40 to *c.* 113 Ma (Debon *et al.*, 1986).

Indian terrain: Four abraded, slightly discordant zircon crystals from the NB10 biotite-K-feldspar gneiss define a discordia line with a precise upper Concordia intercept age of 484 + 3, –2 Ma interpreted as the time of magmatic emplacement of the protolith

Table 2. Single-zircon U–Pb isotopic data

Sample	Weight (μg)	U (ppm)	Th/U$^{(b)}$ (wt)	$Pb^{(c)}_{rad}$ (ppm)	$Pb^{(d)}_{com}$ (pg)	$^{206}Pb/^{204}Pb^{(e)}$	$^{208}Pb/^{206}Pb^{(f)}$	$^{207}Pb/^{235}U^{(f}$	$^{206}Pb/^{238}U^{(f,g)}$	$\rho^{(h)}$	$^{206}PB/^{238}U$ Age $^{(f,g)}$ (Ma)
NB 10:											
z_1	8.3	724	0.53	55.5	2.7	9477	0.1692 ± 3	0.5681 ± 12	0.07260 ± 9	0.89	451.8 ± 6
z_2	12.5	1310	0.48	104	3.8	19549	0.1542 ± 3	0.5988 ± 12	0.07648 ± 10	0.93	475.1 ± 6
z_3	5.8	558	0.61	45.1	4.6	3105	0.2204 ± 4	0.5752 ± 15	0.07353 ± 8	0.74	457.4 ± 5
z_4	10.1	1371	0.52	110	5.1	12439	0.1675 ± 3	0.5988 ± 12	0.07646 ± 10	0.90	475.0 ± 6
NB 93:											
z_1	2.4	229	1.54	3.28	4.8	93.8	0.506 ± 12	0.0674 ± 86	0.01072 ± 7	0.81	68.82 ± 43
z_2	4.1	544	1.53	7.83	4.2	367.4	0.5015 ± 34	0.0706 ± 22	0.01078 ± 3	0.62	69.17 ± 17
z_3	9.6	714	0.64	8.30	3.5	1309	0.2093 ± 13	0.0703 ± 8	0.01075 ± 2	0.42	69.00 ± 14
$z_{4.1(a)}$	4.1	489	0.59	8.51	3.6	570.7	0.1925 ± 26	0.1071 ± 24	0.01630 ± 4	0.46	104.32 ± 28
$z_{4.2(a)}$	2.1	666	0.48	9.56	3.1	398.2	0.1567 ± 38	0.0914 ± 30	0.01385 ± 3	0.72	88.79 ± 18

(a) Fragments from the same grain; (b) calculated from radiogenic $^{208}Pb/^{206}Pb$; (c) radiogenic Pb; (d) total common Pb in analysis (including blank); (e) measured ratios corrected for mass fractionation; (f) ratios corrected for tracer contribution, mass fractionation, laboratory Pb blank (NB10: 1.8 ± 0.9 pg, $^{208}Pb/^{206}Pb = 2.092 \pm 0.050$, $^{207}Pb/^{206}Pb = 0.866 \pm 0.027$, $^{204}Pb/^{206}Pb = 0.0553 \pm 0.0007$; NB93: 3.5 ± 1.5 pg, $^{208}Pb/^{206}Pb = 2.069 \pm 0.041$, $^{207}Pb/^{206}Pb = 0.855 \pm 0.017$, $^{204}Pb/^{206}Pb = 0.0547 \pm 0.0018$; all errors are 2σ) and initial common Pb (NB10: initial total-rock Pb isotopic composition at 484 Ma; NB93: 69 Ma model III (Cumming and Richards, 1975) Pb composition; analytical uncertainties are given at the 95% confidence level and refer to the least significant digits of the corresponding values; (g) ratios and ages corrected for initial disequilibrium in $^{230}Th/^{238}U$, assuming crystallisation from a reservoir with Th/U = 4.04 (NB10: measured total-rock value) and 3.6 (NB93: adopted value), respectively; (h) $^{207}Pb/^{235}U$ versus $^{206}Pb/^{238}U$ correlation coefficient (for further analytical details see Meier and Oberli in Wiedenbeck *et al.*, 1995)

Table 3. Sm–Nd isotope data for NB58 garnets and whole rock

Sample	Weight (mg)	Sm (ppm)	Nd (ppm)	$^{147}Sm/^{144}Nd$	$(2\sigma)^{(1)}$	$^{143}Nd/^{144}Nd$	$(2\sigma)^{(1,2)}$
Whole rock	104.0	12.92	74.06	0.1055	(01)	0.511781	(09)
Grt(1)	7.4	1.14	0.394	1.7461	(79)	0.511967	(60)
Grt(2)	9.2	2.05	4.076	0.3035	(21)	0.511772	(22)
Grt(3)	11.2	1.74	3.489	0.3019	(13)	0.511809	(14)
Grt(4)	16.9	1.30	0.523	1.5038	(37)	0.511908	(37)
Grt(5)	9.0	1.44	0.522	1.6750	(34)	0.511956	(36)

(1) Errors refer to last two digits. (2) $^{143}Nd/^{144}Nd$ normalised to 0.7219. Six replicate analyses of La Jolla Nd standard (5–50 ng) yielded a weighted mean value of 0.511856 ± 0.000005 (95% c.l. external). An excess run-to-run variance component of 1.5×10^{-11} derived from these measurements has been added to the observed within-run variances of the sample measurements

(Fig. 11, Table 2). Most of the euhedral grains show slightly curved crystal edges, a feature attributed to resorption during the Cenozoic metamorphic overprint. This Early Ordovician age further supports the comparison between these rocks and the north Himalayan belt of granitic and gneissic domes (Burg and Chen, 1984). Similar ages have been reported for various Himalayan basement units (e.g., Nanga Parbat, Zeitler *et al.*, 1989; Zanskar, Pognante *et al.*, 1990; "Lesser" Himalaya, Schärer and Allègre, 1983; see also references cited by Debon *et al.*, 1986).

The present-day whole rock ε_{Nd} value of ~16.7 calculated from the Nd data of the NB58 metapelite (Table 3) and values of ~15.2, ~13.5 and ~11.7 obtained for samples NB10, NB12 and NB64, respectively (Oberli *et al.*, unpublished data) conform to the distribution of ε_{Nd} values reported for high Himalayan crystalline rocks and partly overlap with those from ODP Leg 116 sediments (France-Lanord *et al.*, 1993; Galy *et al.*, 1996). Using the parameters given by Farmer and DePaolo (1983) we calculate a model age of ~1770 Ma relative to a depleting mantle for NB58, which represents a minimum age for the oldest components in this metasedimentary rock. This result is similar to protolith ages of ~1850 Ma in the Nanga Parbat region determined from zircon upper Concordia intercept ages (Zeitler *et al.*, 1989).

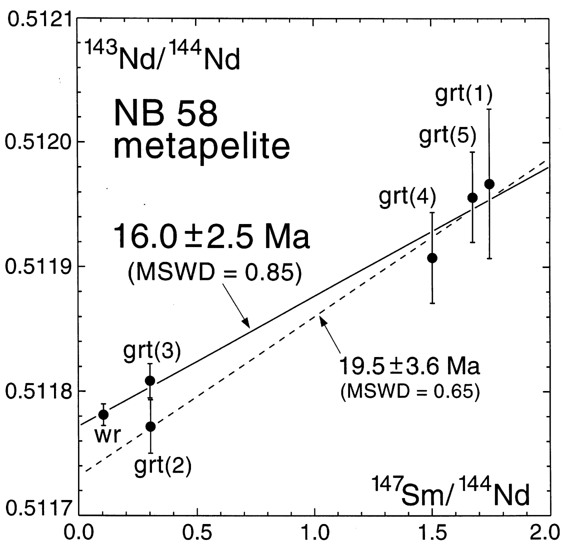

Fig. 12. Sm–Nd isotopic data for the NB58 metapelite sample. An isochron combining garnet analyses 1-3-4-5 and whole rock corresponds to an age of 16.0 ± 2.5 Ma and an initial $^{143}Nd/^{144}Nd$ value of 0.511772 ± 0.000008 (95% c.l. internal). The dashed line linking the "impure" garnet fraction (2) with the data points of purified garnet fractions 1-4-5 yields an older age of 19.5 ± 3.6 Ma and initial $^{143}Nd/^{144}Nd$ of 0.511732 ± 0.000027 (see text).

The presence of meta-igneous rocks of early Ordovician age in a gneiss characterised by an Early to Mid-Proterozoic residence age supports the interpretation that rocks in the core of the Namche Barwa syntaxis are derived from Indian plate protoliths.

High temperature ages

The time of peak metamorphic conditions is constrained by Sm–Nd data obtained on whole rock and five garnet fractions from the NB58 metapelite (Table 3 and Fig. 12), which is similar to and has been collected at the same locality as sample NB24 used for thermobarometry. Garnet fractions 1-3-4-5 have been prepared by careful selection of inclusion-free fragments using a binocular microscope, whereas fraction 2 has been selected to be more representative of the average crystal quality characterized by the presence of tiny inclusions. We note that the data from the former, together with the whole rock, can be fitted by an isochron yielding an age of 16.0 ± 2.5 Ma with MSWD = 0.85 (Fig. 12). Whereas three out of the four garnet fractions cluster at elevated Sm/Nd values and are characterised by low Nd concentrations of 0.39–0.52 ppm, fraction 3 plots close to the whole-rock value and has a relatively high Nd concentration of 3.5 ppm. This suggests a presence in this fraction of components (inclusions) enriched in Nd, which have escaped detection during the handpicking process. The impure garnet fraction 2 has a similarly elevated Nd concentration of 4.1 ppm. A $^{143}Nd/^{144}Nd$ ratio lower than the corresponding whole rock value suggests presence of older mineral phases characterised by low Sm/Nd and high Nd concentration, which have not equilibrated their Nd isotopic composition at the time of metamorphism. A likely candidate is allanite, which is abundant in this rock. A line connecting the "impure" garnet fraction (2) with the data points of purified garnet fractions 1-4-5 would yield an older age of 19.5 ± 3.6 Ma, with MSWD = 0.65 (Fig. 12). In view of these systematical aspects we give preference to the former age and adopt 16.0 ± 2.5 Ma as an estimate for the time of metamorphism.

The numerous xenotime crystals found in the NB12 quartz-feldspar leucosome layer (Fig. 9) are mostly euhedral and show relatively high U contents (1.8–2.5%). The precise U–Th–Pb isotopic results obtained on seven crystals show that they have crystallised during the period 3.9–3.3 Ma, which dates the last anatectic event because (i) they occur within an *in-situ*

Table 4. Fission-track ages on apatites and zircons from Namche Barwa region. ρ_s and ρ_i represent sample spontaneous and induced track densities; $P(\chi^2)$ is the probability of χ^2 for v degrees of freedom where v = (number of crystals −1). All ages are central ages (Galbraith, 1981). $\lambda_D = 1.55125 \times 10^{-10}$. A geometry factor of 0.5 was used. Zeta = 360 ± 5 for CN5 and Durango apatite and 120 ± 8 for CN1 and Fish Canyon tuff zircon. Irradiations were performed at the ANSTO facility, Lucas Heights, Australia

Sample Number	Altitude (m)	Irradiation number	Number of grains counted	Standard track density $\times 10^4$ cm^{-2} (counted)	$\rho_s \times 10^4$ cm^{-2} (counted)	$\rho_i \times 10^4$ cm^{-2} (counted)	$P\chi^2$	Age $\pm 2\sigma$ (Ma)
NB10-apatite	4100	eth-40-7	30	140 (3137)	1.58 (27)	364 (6231)	96	1.1 ± 0.4
NB12-apatite	3400	eth-40-6	38	143 (3137)	0.49 (6)	143 (1745)	42	0.9 ± 0.8
NB64-apatite	2900	eth-40-8	29	137 (3137)	1.06 (13)	243 (3000)	68	1.1 ± 0.6
NB6-apatite	2020	eth71-13	50	149 (2873)	0.256 (8)	131 (4083)	33	0.5 ± 0.4
NB9-apatite	3000	eth71-16	20	145 (2873)	9.5 (117)	301 (3703)	30	8.2 ± 1.6
NB10-zircon	4100	eth-43-25	20	15.8 (1507)	63.0 (430)	687 (4685)	< 5	2.5 ± 0.4
NB64-zircon	2900	eth-43-27	20	15.7 (1507)	49.06 (322)	49.7 (3264)	25	2.6 ± 0.4

leucosome layer of the unaltered migmatitic parent rock; (ii) they are large (up to 350 μm) and very abundant, which is readily seen in thin section. Similarly, a euhedral, transparent green thorite crystal from sample NB64 yielded a precise ^{232}Th/^{208}Pb age of 2.9 Ma. The U–Th–Pb systematics of both the xenotime and the thorite data indicate preservation of an initial isotopic disequilibrium signature in ^{230}Th/^{238}U, which suggests that these ages refer to the times of crystallisation rather than resetting by loss of radiogenic Pb due to thermometamorphic overprint.

Lower temperature ages

Fission track dating was carried out using the external detector method and the zeta approach (Hurford and Green, 1983). Analytical results are given in Table 4. Zircons from altitudes 2900 and 4100 m yield statistically equal ages of 2.6 ± 0.4 and 2.5 ± 0.4 Ma. The closure temperature for zircon is ~250°C (Tagami *et al.*, 1996). Apatite ages from altitudes 2900, 3730 and 4100 m give statistically similar results, 1.1 ± 0.6, 0.9 ± 0.8 and 1.1 ± 0.4 Ma respectively. A rapid cooling rate enhanced by the advection of the geotherms and the presence of high relief is postulated. Estimates for closure temperatures in apatites fall in the range 75–125°C for cooling rates between 1 and 100°C/Myr (Wagner and Reimer, 1972; Haack, 1977; Gleadow and Lovering, 1978). The upper level of 125°C is used here.

In order to estimate the regional age pattern away from the antiform, samples NB9 and NB6 (located Fig. 1) were analysed. NB9 yielded an apatite age of 8.2 ± 1.6 Ma. The mean track length is 14.49 ± 0.21 μm (σ = 1.58 μm). This age fits one of the unlocated four groups of fission track ages reported by Zhong and Ding (1996b) and suggests that fast unroofing has been active from at least this time. NB6 apatite yielded an unexpectedly young age of 0.5 ± 0.4 Ma. It was sampled in an area where active faulting along both the Jiali-Parlung fault and the sinistral bounding fault is pervasive and hot springs are numerous. Clearly this then cannot be treated as a regionally relevant age; it may have been reset by the later and local hydrothermal and/or tectonic recent events.

Summary

Garnet growth under peak metamorphic conditions in the centre of the syntaxis occurred at *c.* 16 Ma, and therefore predates by *c.* 12 Ma exhumation dated by xenotime in migmatitic leucosomes. Similar offsets between times of burial and uplift have been reported from other Himalayan areas (Vance *et al.*, 1997). The limited range of ages from 3.9 to 2.8 Ma displayed by xenotime and thorite and the lack of age variation with altitude for the fission-track cooling ages of *c.* 2.5 Ma (zircon) and *c.* 1.1 Ma (apatite) are taken as evidence for intense tectonic activity accompanying very rapid cooling-exhumation (100°C.Myr^{-1} or more, Fig. 13) of rocks that were about 30 km deep and still anatectic about 4 Myr ago. We will now try to specify

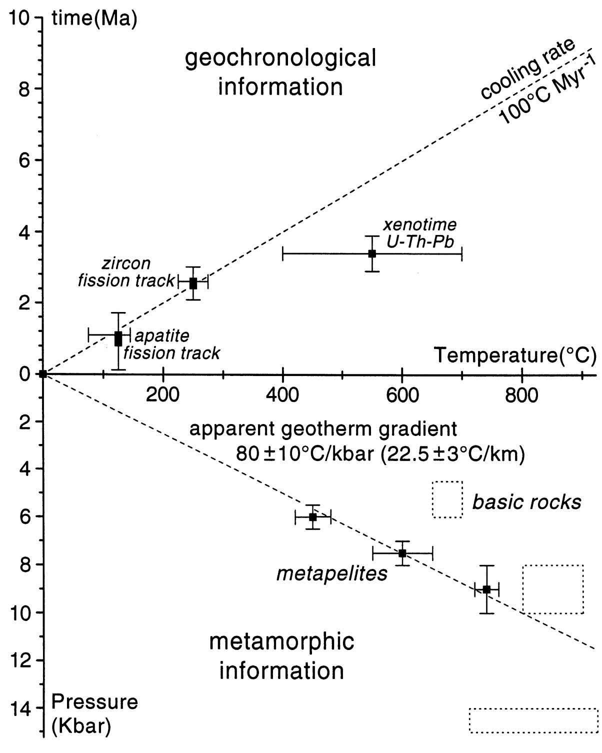

Fig. 13. Top = cooling history as implied from fission-track and U–Pb versus corresponding closing temperatures, compared to the decompression history (below) inferred from metamorphic parageneses. Dashed squared are successive metamorphic conditions in mafic rocks from Zhong and Ding (1996).

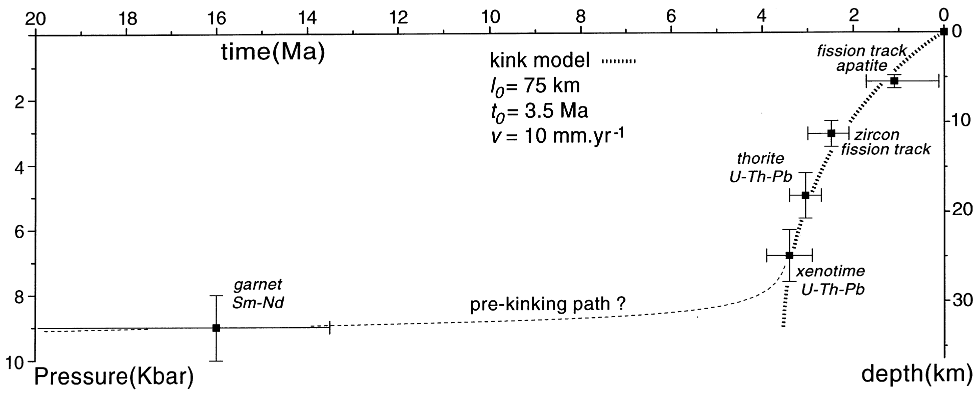

Fig. 14. Decompression history fitted by a folding-kinking model with fold amplification balanced by erosion.

the dynamic history of the core of the Namche Barwa antiform.

Rapid erosion of growing crustal folds

The samples used in the present work come from one short section within the core of the antiform, without any major faults between them (Figs 1 and 4). Therefore we assume that they all have undergone the same bulk history, related to that of the deepest parts of the antiform. Petrological calculations (Fig. 13) do not yield syn-decompression heating as expected from thermal-exhumation models with 1D heat transfer and linear erosion rates (England and Thompson, 1984; Davy *et al.*, 1989). We presume that this is due to very fast exhumation as much as to lateral heat transfer that tends to attenuate the "deformation" of the geothermal gradient (Gaudemer *et al.*, 1988). In effect, the Namche Barwa antiform is as wide as deep (30 to 40 km) and lateral heat transfer of the same order as vertical heat transfer can be forecast (see a similar discussion in Koons, 1987). Because the thermal-exhumation history is very fast (less than 4 Myr from migmatites to exposure) we may combine petrological and geochronological information to deduce the pressure-time path, with special attention to the calculation of error bars that may be very large when extrapolating temperatures to pressures (Fig. 13). The resulting curve (Fig. 14) readily reveals that the exhumation rate decreased from *c.* 10 mm yr^{-1} between 3.5 and 3.2 Ma to 3–5 mm yr^{-1} since 2.2 Ma until the present time.

Our prejudice is that the metamorphic history is necessarily related to the compressional deformation kinetics defined by structural arguments. In order to check the plausibility of our interpretation, several calculations have been designed to plot uplift rates during progressive horizontal shortening (Fig. 15). First of all, a process that would be described by homogeneous shortening generates an exponentially accelerating exhumation, which is in contradiction with the slowing down exhumation rate mentioned above. Since the

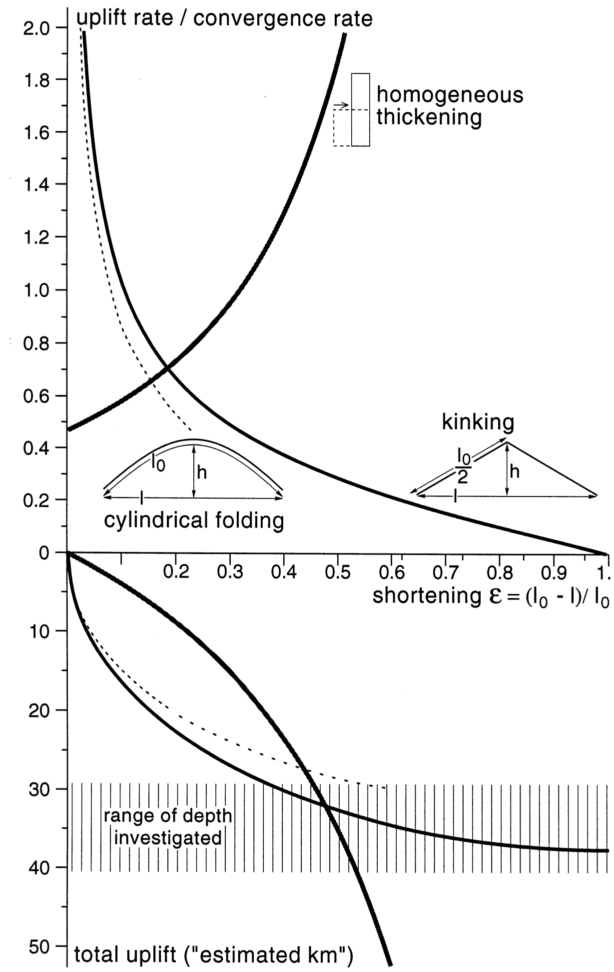

Fig. 15. Theoretical models investigated to understand structurally controlled exhumation rates and their variation. Some sort of homogeneous thickening can be readily excluded (the curve, top part, begins at h/l with h the initial depth, i.e. thickness of the eroded layer (35 km) and l_0 the initial length (75 km). Note that cylindrical folding leads to nearly no amplification after a relatively small shortening strain.

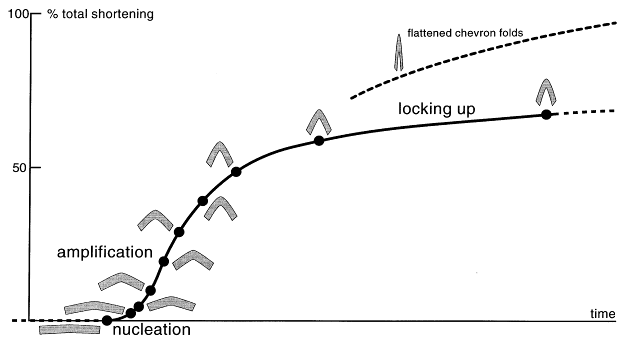

Fig. 16. Development of chevron folds under constant end load (adapted from Ramsay, 1974; Cobbold, 1976b).

Namche Barwa syntaxis is a large-scale antiform, we have decided to relate the data points of Fig. 14 to the amplitude history during fold growth. Precisely, very fast uplift/exhumation rates may fit rapid amplification recorded by experimental and numerical studies of buckle folding (Fig. 16, Biot, 1961; Sherwin and Chapple, 1968; Ramsay, 1974). Moreover, decaying decompression rates are consistent with the fact that amplitude growth significantly slows for large amounts of shortening (Cobbold, 1976b; Parrish *et al.*, 1976; Lewis and Williams, 1978). For the rocks investigated, exhumed from >10 kbars, i.e. from 30–40 km, folding-related uplift is sufficiently approximated by a kink model (Fig. 15). The analytical solution is simple. Both limbs are equal, and half of the initial length l_0 of a considered layer. Taking time as t with kinking beginning at t_0 under a horizontal convergence velocity v, the length is a time function $l_{(t)} = l_0 + v(t - t_0)$ as well as h, the height of the kink $h_{(t)} = \frac{1}{2}\sqrt{(l_0\ \ )^2 - l(t)^2}$. However, petrological calculations give us a pressure equated with a depth. Therefore, we need to know the z-depth history of rocks sampled now in the core of the kink. The depth history is given by

$$z_{(t)} = \frac{1}{2}\left[\sqrt{(l_0)^2 - (l_0 - vt_0)^2} - \sqrt{(l_0)^2 - [l_0 - v(t - t_0)]^2}\right].$$

Mechanically, kinking represents an end member solution for very anisotropic systems where layer-parallel stretching is impossible, but it suits our problem because the bluntness of folds increases with strain (Cobbold, 1976a). The calculation that best fits the decompression curve (Fig. 14) implies regionally consistent average parameters of initial length $l_0 = 75$ km, starting growth of fold at $t_0 = 3.5$ Ma, and convergence velocity $v \sim 10\ \mathrm{mm \cdot yr^{-1}}$, about half the rate estimated for the Himalayas (Molnar 1984, 1987). Note that 3.5 Ma is the youngest age for the beginning of crustal scale folding but some time span is often observed in mechanical description of fold initiation, usually corresponding to some stable shortening of the layers under lateral compression. Therefore, this age must not be taken as the onset of convergence. At about 50% of finite shortening (to reach the *c.* 35 km present-day width of the antiform), the model consistently predicts a current uplift rate of 3–5 mm $\mathrm{yr^{-1}}$.

The decompression in the folds is caused either by erosion or by tectonic denudation. We have seen little evidence for dramatic tectonic denudation. Conversely, impressive land slides demonstrate that uplift and correlative erosion are still very active. The average slope of the Yalu Tsangpo-Brahmaputra is rather steep, *c.* 30 $\mathrm{m \cdot km^{-1}}$ from Pai (near NB64 on Fig. 1) at 2900 m to 700 m near Medog, in its great U-turn where it has incised terraces by more than 350 m. Although a quantitative estimation is difficult, the erosion rate has been necessarily fast to produce the "world's deepest valley" (*The Guinness Book of Records*) between the Namche Barwa (at 7756 m) and the Giala Peri (7281 m). Therefore, we consider that exhumation of *c.* 10 mm $\mathrm{yr^{-1}}$ was mostly due to efficient erosion of an antiformal hinge region during compressional folding. This would not be exceptional because a similar erosion rate is reported in the tectonically active ranges of Southeast Alaska where glaciers play a key erosional role (Hallet *et al.*, 1996). Note that in the Namche Barwa case we may intuitively conceive that erosion of the hinge region has weakened it, hence concentrating further folding strain in the hinge more than on the limbs, which is a further argument to consider kinking/chevron folding as a satisfactory and sufficient approximation.

Discussion

Our field data, accurate dating and modelling establish that the Namche Barwa syntaxis is a fast-growing, post-collision arcuation of Himalayan trends. It is a large, dominantly northeast plunging antiform within the core of which Indian plate gneisses have been exhumed from below the Transhimalayan plutonic belt over the last 4 Ma. The youthful geomorphology suggests that uplift and concurrent exhumation are continuing to produce the Namche Barwa syntaxis, which involves a combination of folding and faulting in a convergent environment.

The thermomechanical evolution of the Namche Barwa syntaxis presents remarkable similarities with the Nanga Parbat syntaxis at the western end of the Himalayas (Zeitler *et al.*, 1982; Coward *et al.*, 1986; Zeitler *et al.*, 1989; Treloar *et al.*, 1991; Smith *et al.*, 1992; Burbank *et al.*, 1996; Winslow *et al.*, 1996). Both Himalayan syntaxes straddle the same Neogene time span, which links their growth to the uplift that produced Tibet in the last few million years (Molnar *et al.*, 1993). The bend of regional strikes around the Nanga Parbat area links the Ladakh to the Kohistan arc systems. Symmetrically, the Transhimalayan plutonic belt (also Lhasa block, Burg *et al.*, 1983) is geographically and geologically linked, around the Namche Barwa (our observations and Zheng and Chang, 1979), to the diorite–granodiorite complex that extends further Southeast into India (the so-called Mishmi granodiorites of Nandy, 1976 and Acharyya, 1980; the Lohit plutonic complex of Thakur, 1986) and Burma. The Namche Barwa antiform is the most hinterland structure of the complex and buckled Assam syntaxis (Wadia, 1957; Kumar, 1980; Singh, 1993), just as the Nanga Parbat stands as a hinterland fold with respect to the Hazara–Kashmir syntaxis of northern Pakistan (Bossart *et al.*, 1988). The NW–SE trending western boundary of the Mishmi Hills plutonic complex is a Late Cenozoic thrust over imbricated low- and high-grade metasediments with isolated occurrences of serpentinites and mafic–ultramafic rocks (Dhoundial *et al.*, 1976) that represent dismembered ophiolites (Thakur, 1986). Their continuation is found further south in Burma (the Arakran-Chin ophiolites of Goosens, 1978). Stretching and mineral lineations in the contact zone are reported to strike NNE, with shallow plunges (Thakur and Jain, 1975). Accordingly, we contend and agree with some authors (e.g. Thakur, 1986) that the western boundary of the Mishmi plutonic complex is the continuation of the Tethyan Yalu Tsangpo suture.

Acknowledgements—This work is supported by the ETH-Zürich (Projekt 1-20-888-94). P. Davy is funded by the French CNRS and Dia Zhizhong by the Chinese Academy of Sciences in Chendu. The authors would like to thank Suz-Chung Ko for valuable help in deciphering the Chinese literature and Yang Hsuanlin for his efficient assistance with field work and logistics. We would also like to thank D. Vance for sharing his experience in garnet Sm–Nd analytics with us, H. Derksen for carrying out mineral separation and J. Connolly for his help in thermobarometric calculations. Discussions with A. Thompson, C. Teyssier and L. Ratschbacher and detailed review by P. Zeitler were very helpful.

REFERENCES

Acharyya S. K., (1980) Structural framework and tectonic evolution of the Eastern Himalaya. *Himalayan Geology* **10**, 412–439.

Allègre C. J. and 34 co-authors, (1984) Structure and evolution of the Himalayan–Tibet orogenic belt. *Nature* **307**, 17–22.

Armijo R., Tapponnier P., Mercier J. L. and Han T-L., (1986) Quaternary extension in Southern Tibet: Field observations and tectonic implications. *Journal of Geophysical Research* **91**(B14), 13,803–13,872.

Biot M. A., (1961) Theory of folding of stratified viscoelastic media and its implications in tectonics and orogenesis. *Geological Society of America Bulletin* **72**, 1595–1620.

Bossart P., Dietrich D., Greco A., Ottiger R. and Ramsay J. G., (1988) The tectonic structure of the Hazara-Kashmir Syntaxis, Southern Himalayas, Pakistan. *Tectonics* **7**(2), 273–297.

Burbank D. W., Leland J., Fielding E., Anderson R. S., Brozovic N., Reid M. R. and Duncan C., (1996) Bedrock incision, rock uplift and threshold hillslopes in the northwestern Himalayas. *Nature* **379**, 505–510.

Burg J-P., (1991) Syn-migmatization way-up criteria. *Journal of Structural Geology* **13**(6), 617–623.

Burg J-P. and Chen G. M., (1984) Tectonics and structural zonation of southern Tibet, China. *Nature* **311**, 219–223.

Burg J-P., Davy P., Nievergelt P., Oberli F., Seward D., Diao Z. and Meier M., (1997) Exhumation during crustal folding in the Namche-Barwa syntaxis. *Terra Nova* **9**(2), 53–56.

Burg J-P., Leyreloup A., Girardeau J. and Chen G. M., (1987) Structure and metamorphism of a tectonically thickened continental crust: the Yalu Tsangpo suture zone. *Philosophical Transactions of the Royal Society of London* **A321**, 67–86.

Burg J-P., Proust F., Tapponnier P. and Chen G. M., (1983) Deformation phases and tectonic evolution of the Lhasa block (southern Tibet, China). *Eclogae Geologicae Helvetiae* **76**(3), 643–665.

Chang C-F., Zheng X-L. and Pan Y-S., (1977) The geological history, tectonic zonation and origin of uplifting of the Himalayas. *Institute of Geology, Academia Sinica* , 1–17.

Chang C. G., Lio H. H., Wang T. W., Yang H. X. and Hu B. Z. (1992) *Geology of the Namche Barwa region*. Academia Sinica, 185 p. 86 photographic plates (in Chinese).

Cobbold P., (1976a) Mechanical effects of anisotropy during large finite deformations. *Bulletin de la Société géologique de France* **18**, 1497–1510.

Cobbold P. R., (1976b) Fold shapes as functions of progressive strain. *Philosophical Transactions of the Royal Society of London* **A283**, 129–138.

Connolly J. A. D., (1990) Calculation of multivariable phase diagrams: An algorithm based on generalized thermodynamics. *American Journal of Science* **290**, 666–718.

Coward M. P., Windley B. F., Broughton R. D., Luff I. W., Petterson M. G., Pudsey C. J., Rex D. C. and Khan M. A., (1986) Collision tectonics in the NW Himalayas. *Geological Society Special Publication* **19**, 203–219.

Cumming G. L. and Richards J. R., (1975) Ore lead isotope ratios in a continuously changing earth. *Earth and Planetary Science Letters* **28**, 155–171.

Davy P., Guérin G. and Brun J-P., (1989) Thermal constraints on the tectonic evolution of a metamorphic core complex (Santa Catalina Mountains, Arizona). *Earth and Planetary Science Letters* **94**, 425–440.

Debon F., Le Fort P., Sheppard S. M. F. and Sonet J., (1986) The four plutonic belts of the Transhimalayan-Himalaya: a chemical, mineralogical, isotopic and chronological synthesis along a Nepal section. *Journal of Petrology* **27**(1), 219–250.

Dewey J. F., Shackleton R. M., Chang C. F. and Sun Y. Y., (1988) The tectonic evolution of the Tibetan Plateau. *Philosophical Transactions of the Royal Society of London* **A327**, 379–413.

Dhoundial D. P., Santra D. K. and Dange M. N., (1976) A new look at the stratigraphic and tectonic importance of Tdding limestone and serpentinite in Lohit District. *Geological Survey of India, Miscellaneous Publication* **24**(2), 368–378.

England P. C. and Thompson A. B., (1984) Pressure–temperature–time paths of regional metamorphism I. Heat transfer during the evolution of regions of thickened continental crust. *Journal of Petrology* **25**(4), 894–928.

Etchecopar A., Vasseur G. and Daignières M., (1981) An inverse problem in microtectonics for the determination of stress tensors from fault striation analysis. *Journal of Structural Geology* **3**(1), 51–65.

Farmer G. L. and DePaolo D. J., (1983) Origin of Mesozoic and Tertiary granite in the western United States and implications for pre-Mesozoic crustal structure. 1. Nd and Sr isotopic studies in the geocline of the northern Great Basin. *Journal of Geophysical Research* **88**, 3379–3401.

France-Lanord C., Derry L. and Michard A. (1993) Evolution of the Himalayas since Miocene time: isotopic and sedimentological evidence from the Bengal Fan. In *Himalayan Tectonics*. (Edited by Treloar P. J. and Searle M. P., **74**, pp. 603–621. Geological Society Special Publication, London.

Galbraith R. F., (1981) On statistical models for fission track counts: reply. *Mathematical Geology* **13**, 485–488.

Galy A., France-Lanord C. and Derry L. A., (1996) The Late Oligocene–Early Miocene Himalayan belt: constraints deduced from isotopic composition of Early Miocene turbidites in the Bengal Fan. *Tectonophysics* **260**, 109–118.

Gansser A., (1966) The Indian Ocean and the Himalayas. A geological interpretation. *Eclogae geologicae Helvetiae* **59**(2), 831–848.

Gansser A., (1980) The significance of the Himalayan suture zone. *Tectonophysics* **62**, 37–52.

Gansser A., (1991) Facts and theories on the Himalayas. *Eclogae geologicae Helvetiae* **84**(1), 33–59.

Gaudemer Y., Jaupart C. and Tapponnier P., (1988) Thermal control on post-orogenic extension in collision belts. *Earth and Planetary Science Letters* **89**, 48–62.

Gleadow A. J. W. and Lovering J. F., (1978) Thermal history of granitic rocks from western Victoria: a fission track dating study. *Journal of the Geological Society of Australia* **25**, 323–340.

Goosens P. J. (1978) The metallogenic provinces of Burma: their definitions, geologic relationships and extension into China, India and Thailand. In *Third Regional Conference on Geology and Mineral Resources of Southeast Asia*. (Edited by Nutalaya P.) **3**, pp. 431–492. Asian Institute of Technology, Bangkok.

Group of K–Ar Geochronology Institute of Geology Academia Sinca, (1979) K–Ar dating and division of the Himalayan movement in southern Xizang. *Scientia Geologica Sinica* **1**, 13–21.

Haack U., (1977) The closing temperature for fission track retention in minerals. *American Journal of Science* **277**, 450–464.

Hallet B., Hunter L. and Bogen J., (1996) Rates of erosion and sediment evacuation by glaciers: A review of field data and their implications. *Global and Planetary Change* **12**, 213–235.

Harrison T. M., Duncan I. and McDougall I., (1985) Diffusion of ^{40}Ar in biotite: temperature, pressure and compositional effects. *Geochimica Cosmochimica Acta* **49**, 2461–2468.

Holt W. E., Ni J. F., Wallace T. C. and Haines A. J., (1991) The active tectonics of the Eastern Himalayan Syntaxis and surrounding regions. *Journal of Geophysical Research* **96**(B9), 14,595–14,632.

Hurford A. J. and Green P. F., (1983) The zeta age calibration of fission-track dating. *Isotope Geoscience* **1**, 285–317.

Institute of Geology Mineral Resources Chinese Academy of Geological Sciences (1988) Geological map of Qinghai-Xizang (Tibet) plateau and adjacent areas. 1:1 500 000. *Explanatory note*. Geological Publishing House, Chengdu, notice Pages, 11.

Koons P. O., (1987) Some thermal and mechanical consequences of rapid uplift: an example from the southern Alps, New Zealand. *Earth and Planetary Science Letters* **86**, 307–319.

Kumar S., (1980) Geodynamic interpretation of the Tuting–Dewangiri lineament in the eastern Himalayas. *Himalayan Geology* **10**, 403–411.

Leake B. E., (1978) Nomenclature of amphiboles. *Mineralogical Magazine* **42**, 533–563.

Lewis R. W. and Williams J. R., (1978) A finite-element study of fold propagation in a viscous layer. *Tectonophysics* **44**, 263–283.

Liu Y. H., (1984) An outline of the geological features in the Mt Namjagbarwa region. *Mountain Research* **2**(3), 204–211 (in Chinese).

Liu Y. and Zhong D., (1997) Petrology of high-pressure granulites from the eastern Himalayan syntaxis. *Journal of Metamorphic Geology* **15**, 451–466.

Molnar P., (1984) Structure and tectonics of the Himalayas: Constraints and implications of geophysical data. *Annual Reviews of Earth and Planetary Sciences* **12**, 489–518.

Molnar P., (1987) Inversion of profiles of uplift rates for the geometry of dip-slip faults at depth, with examples from the Alps and the Himalayas. *Annales Geophysicae* **5B**(6), 663–670.

Molnar P., England P. and Martinod J., (1993) Mantle dynamics, uplift of the Tibetan plateau, and the Indian monsoon. *Review of Geophysics* **31**(4), 357–396.

Nandy D. R., (1976) The Assam Syntaxis of the Himalayas—A re-evaluation. *Geological Survey of India* **24**(2), 364–367 (Miscellaneous Publication).

Oberli F., Meier M., Seward D., Burg J-P., Nievergelt P., Davy P., Maurin J-C. and Diao Z-Z., (in prep.) "Age" vs process. Interpretation of Pliocene high-resolution U–Th–Pb isotope data for the Namche Barwa syntaxis (SE) to be submitted at Earth and Planetary Science Letters.

Parrish D. K., Krivz A. L. and Carter N. L., (1976) Finite element folds of similar geometry. *Tectonophysics* **32**, 183–207.

Pognante U., Castelli D., Benna P., Genovese G., Oberli F., Meier M. and Tonarini S., (1990) The crystalline units of the high Himalayas in the Lahul-Zanskar region (northwest India): metamorphic-tectonic history and geochronology of the collided and imbricated Indian plate. *Geological Magazine* **127**, 101–116.

Ramsay J. G., (1974) Development of chevron folds. *Geological Society of America Bulletin* **85**(11), 1741–1754.

Ratschbacher L., Frisch W., Chen C. S. and Pan G. T., (1992) Deformation and motion along the southern margin of the Lhasa Block prior to and during the India–Asia collision. *Journal of Geodynamics* **16**(1/2), 21–54.

Schärer U. and Allègre C. J., (1983) The Palung granite (Himalayas); high-resolution U–Pb systematics in zircon and monazite. *Earth and Planetary Science Letters* **63**, 423–432..

Sherwin J. A. and Chapple W. M., (1968) Wavelengths of single layer folds: a comparison between theory and observation. *American Journal of Science* **266**, 167–179.

Singh S., (1993) Geology and tectonics of the Eastern Syntaxial Bend, Arunachal Himalaya. *Journal of Himalayan Geology* **4**(2), 149–163.

Smith H. A., Chamberlain C. P. and Zeitler P. K., (1992) Documentation of Neogene regional metamorphism in the Himalayas of Pakistan using U–Pb in monazite. *Earth and Planetary Science Letters* **113**(1/2), 93–105.

Tagami T., Carter A. and Hurford A. J., (1996) Natural long-term annealing of the zircon fission-track system in Vienna Basin deep borehole samples: constraints upon the partial annealing zone and closure temperature. *Chemical Geology* **130**, 147–157.

Thakur V. C., (1986) Tectonic zonation and regional framework of Eastern Himalaya. *Sciences de la Terre* **47**, 347–360.

Thakur V. C. and Jain A. K., (1975) Some observations of deformation metamorphism and tectonic significance of the rocks of some parts of the Mishmi Hills, Lohit District (NEFA) Arunachal Pradesh. *Himalayan Geology* **5**, 339–364.

Treloar P. J., Potts G. J., Wheeler J. and Rex D. C., (1991) Structural evolution and asymmetric uplift of the Nanga Parbat syntaxis, Pakistan Himalayas. *Geologische Rundschau* **80**(2), 411–428.

Vance D., Prince C. I., Anczkiewicz R. and Harris N., (1997) The timing and rate of prograde metamorphism in the Himalayan orogen. *Terra Nova* **64**, .

Wadia D. N., (1931) The syntaxis of the northwest Himalayas: its rocks, tectonics and orogeny. *Records of the Geological Survey of India* **65**, 189–220.

Wadia D. N. (1957) *Geology of India*. Macmillan Co., London, p. 425.

Wagner G. A. and Reimer G. M., (1972) Fission track tectonics: the tectonic interpretation of fission track apatite ages. *Earth and Planetary Science Letters* **14**, 263–268.

Wang T. W., (1985) Metamorphism generalization of the Mt Namjagbarwa region. *Mountain Research* **3**(4), 196–204 (in Chinese).

Wang T. W., (1993) The petrology and metamorphism of the Aniqiao ductile deformation and metamorphic belt in Moto County. *Geology of Tibet* **1**(9), 77–85 (in Chinese).

Wiedenbeck M., Allé P., Corfu F., Griffin W. L., Meier M., Oberli F., von Quadt A., Roddick J. C. and Spiegel W., (1995) Three natural zircon standards for U–Th–Pb, Lu–Hf, trace element and REE analyses. *Geostandards Newsletter* **19**, 1–23.

Winslow D. M., Zeitler P. K., Chamberlain C. P. and Williams I. S., (1996) Geochronologic constraints on syntaxial development in the Nanga Parbat region, Pakistan. *Tectonics* **15**(6), 1292–1308.

Wu Z-M., (1992) Distribution of seismicity and active faults in Tibetan Plateau. *Journal of Seismological Research* **15**(2), 210–218.

Zeitler P. K., Johnson N. M., Naeser C. W. and Tahirkheli A. K., (1982) Fission-track evidence for Quaternary uplift of the Nanga Parbat region, Pakistan. *Nature* **298**, 255–257.

Zeitler P. K., Sutter J. F., Williams I. S., Zartman R. and Tahirkheli R. A. K., (1989) Geochronology and temperature history of the Nanga Parbat–Haramosh Massif, Pakistan. *Geological Society of America* , 1–22 (Special Paper 232).

Zhang Y-Q., Dai T-M. and Hong A-S., (1981) Isotopic geochronology of granitoid rocks in southern Xizang plateau. In *Proc. Symp. Qinghai Xizang (Tibet) plateau*. Geological, Ecological studies of Qinghai-Xizang plateau, **1**, pp. 483–495. Science press, Beijing, (Beijing, China).

Zhang Z. G., Zhao J. S. and Cheng C. L., (1987) Isotopic dating of the metamorphic rocks in the Namjagbarwa region. *Science Bulletin* **2**, 133–137 (in Chinese).

Zheng X. L. and Chang C. F., (1979) A preliminary note on the tectonic features of the lower Yalu-Tsangpo river region. *Scientia geologica Sinica*, **2**, 116–126 (in Chinese).

Zhong D. L. and Ding L., (1996a) Discovery of high-pressure basic granulites in Namjagbarwa area, China. *Chinese Science Bulletin* **41**(1), 87–88.

Zhong D. L. and Ding L., (1996b) Rising process of the Qinghai-Xizang (Tibet) plateau and its mechanism. *Science in China* **39**(4), 369–379.